Measuring forests with dual wavelength lidar: A simulation study over topography

Steven Hancock [a,c,*], Philip Lewis [b,c], Mike Foster [d], Mathias Disney [b,c], Jan-Peter Muller [e,c]

[a] Department of Geography and Space and Climate Physics, UCL, United Kingdom
[b] Department of Geography, UCL, United Kingdom
[c] NCEO, United Kingdom
[d] Hovemere ltd., United Kingdom
[e] Department of Space & Climate Physics, UCL, United Kingdom

ABSTRACT

Accurate measurements of biophysical parameters are essential for understanding the distribution and dynamics of global vegetation, which exerts an influence on the carbon cycle and atmospheric circulation. Spaceborne, large footprint lidar has been shown to be a valuable tool. It is capable of measuring denser forests than other existing remote methods.

However large-footprint lidar struggles to separate ground and canopy signals over topography and in the presence of short vegetation. This prevents the physically-based measurement of forest properties (such as canopy height and cover) at an acceptable accuracy (sub 10 m root mean square error for height) without the use of external data. The necessary external datasets are not yet available at a global scale at high accuracy.

In this paper the issues of measuring forests with large-footprint, monochromatic lidar are presented. A number of subtle effects, such as shadows beneath crowns, can hamper the reliable measurement of forests. It is proposed that a dual wavelength lidar will allow the separation of canopy from ground returns in these situations and so allow the physically-based measurement of forests.

An initial algorithm is developed and tested with Monte-Carlo ray tracer simulations as a proof of concept. Some refinements are needed to make the method more robust, but the initial form was found to determine the start of the ground return over steep slopes and a range of forest densities, canopy heights and vertical structures with a root mean square error (RMSE) of 2.7 m and mean bias of 67 cm for canopies with covers below 99%. This resulted in canopy height RMSE of 2.88 m with a bias of −23 cm. Such a system will allow measurement of a much broader range of forests than is possible with monochromatic lidar and could form a second generation spaceborne lidar mission.

1. Introduction

Ecological models require accurate biophysical parameters of vegetation on a global scale to ensure realistic representations of growth and atmospheric interactions (Hurtt et al., 2004; Clark et al., 2011). Biomass, leaf area index (LAI) and tree height are some of the most important biophysical parameters (Williams, 1996) whilst satellites are the only way to achieve globally consistent data-sets and allow the temporal resolution necessary for environmental modelling and monitoring

schemes. Currently there is some disagreement on the biomass contained within forests and the spatial distribution of that biomass (Houghton et al., 2001) due to the sparsity of field data, saturation of remote passive optical and radar measurements (Myneni et al., 2002; Waring et al., 1995).

It has been shown that lidar offers a number of advantages over remote passive optical and radar measurements. In particular they have been shown to be capable of measuring far denser canopies (Hofton et al., 2002). In addition, lidar's range resolved nature allows direct measurement of variables, such as canopy height and vertical element distribution, impossible to capture directly with other remote sensing instruments. This avoids some of the methodological issues of other approaches (Dubayah and Drake, 2005). Such direct measures can be ingested into models and so help make errors more tractable (Hurtt et al., 2004). This would greatly help our understanding of the world's forests and its interaction with the carbon cycle and atmospheric circulation (Lefsky, 2010).

* Corresponding author. Now at: Department of Geography, University of Swansea and the National Centre for Earth Observation (NCEO), United Kingdom. Tel.: +44 792602959.
E-mail addresses: stevenhancock2@gmail.com, steven.hancock@dur.ac.uk (S. Hancock).
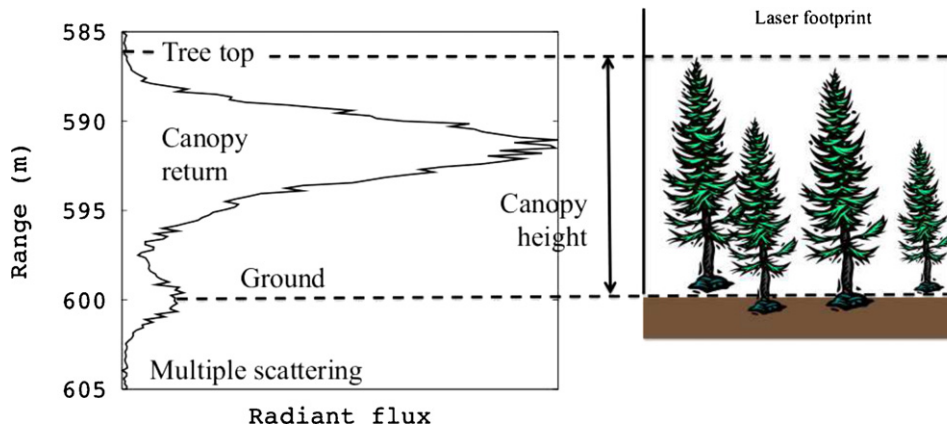
Fig. 1. Simulated 30 m footprint lidar waveform over a forest with features marked.

1.1. Forests and spaceborne lidar

Physically-based measurements with lidar rely on the ground and canopy returns being identifiable. Fig. 1 illustrates a simple case in which there is a clear gap in the waveform between the ground and canopy. There need not be a clear gap, but there must be some identifiable feature to allow a separation. Most previous studies have decomposed the waveform into Gaussians and used these to determine the ground position; either the last Gaussian (lowest elevation), the brightest of the last two (Brenner et al., 2003; Hofton et al., 2000; Chen, 2010) or the average position of the last two (Rosette et al., 2010).

This requires that there be a clear point of inflection between the ground and canopy returns in order to fit a separate function to the canopy and ground. Topography and low lying vegetation (either understory or canopy elements) can complicate this. Fig. 2 shows an example over steep (30° slope) topography. There is no clear feature to allow separation by function fitting and so Gaussian decomposition is unlikely to produce accurate results. This increased error is reported in the literature (Harding and Carabajal, 2005; Lefsky et al., 2007; Los et al., 2011).

In some canopies there may be a feature separating the higher canopy returns from the ground, but the "ground" return may still contain signal from low lying vegetation, as in Fig. 3. Gaussian decomposition will not always be able to separate this low vegetation from the ground. This low lying vegetation can form a significant part of a biome's photosynthetically active material (Chen and Cihlar, 1996) and should not be ignored.

A more subtle effect can be caused by shadows. In forests, canopy elements are clumped into tree crowns, branches and shoots. These will cast discrete shadows in the laser footprint, reducing the intensity of the ground return directly beneath a crown. On sloping ground these shadows will be at a certain range in the waveform and so the ground return intensity will be reduced at certain ranges, as illustrated in Fig. 4. Generally the ground return is assumed to be Gaussian (Hyde et al., 2005), however shadows will take "bites" out of this regular shape, leading to multi-peaked ground returns (Fig. 4). In such an instance multiple Gaussians would be fitted to the ground return so that the centre of the lowest (in terms of elevation) Gaussian does not correspond to the centre of the ground. The drop in intensity due to the shadow could mistakenly be interpreted as the separation between the ground and canopy, leading to an inaccurate height estimate. This may explain why sometimes the most intense of the lowest (in terms of elevation) Gaussian is closer to the ground than the lowest (in terms of elevation), as reported in Hofton et al. (2002) and Chen (2010).

The height variation of the ground within a footprint is proportional to the footprint diameter. Therefore the smaller the footprint the smaller the effect of topography. However, the continuous coverage of a lidar measurement (whether a single footprint or an aggregate of many small adjacent footprints) must be large enough to ensure that some returns are received from tree tops and some from the ground (Zimble et al., 2003); corresponding to a circular footprint of between 10 m and 30 m diameter. There is a proposal for an instrument that can achieve this coverage with an array of small footprints, called LIST (National Academy of Sciences, 2007),
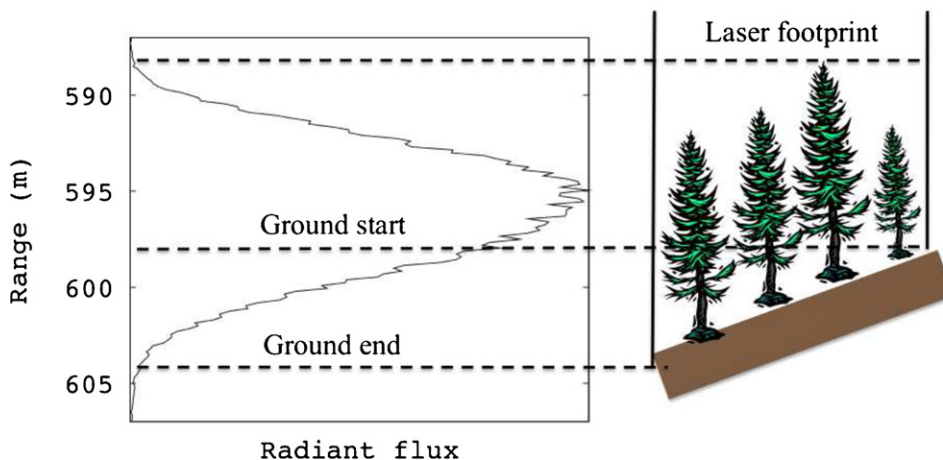

Fig. 2. Illustration of topographic blurring of a simulated 30 m footprint on a 30° slope.
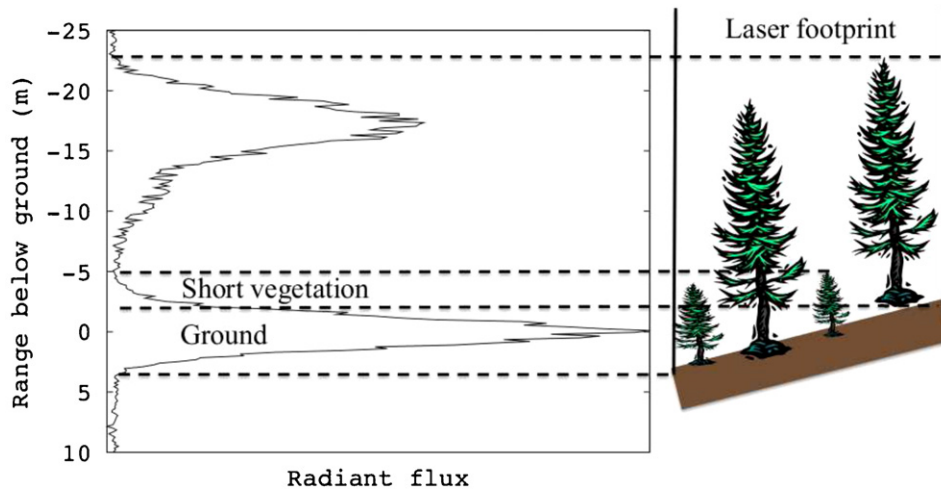
Fig. 3. Effect of understory on a simulated 30 m footprint waveform over a bimodal forest on a 12° slope.

but it is still in the very early stages of development. Therefore, as spaceborne lidar looks set to remain large-footprint for the foreseeable future (when national budgets allow it to be considered again) a reliable method for separating the ground and canopy returns is needed.

1.2. Review of the state of the art

There have been a number of attempts to correct large-footprint lidar returns for topography using a variety of methods and additional datasets. These ranged from empirically relating lidar metrics to ground data in a distinctly non-physical manner (Lefsky et al., 2007) through to entirely physically-based methods that rely on external topographic data (Harding and Carabajal, 2005; Rosette et al., 2008).

The fully empirical corrections of Lefsky et al. (2007) will always be site specific and so unsuitable for a global product (though a global product has been created (Lefsky, 2010), doubts as to its accuracy have been raised (Los et al., 2011)). The physically-based methods of Harding and Carabajal (2005) and Rosette et al. (2008) used an external digital elevation model (DEM) to predict the shape of the ground return and overlaid that with the waveform to separate the ground and canopy returns. Rosette et al. (2008) achieved a canopy height accuracy (root mean square error, RMSE) of 2.5 m using a 10 m horizontal resolution DEM provided by the UK

Ordnance Survey for the 65 m footprint ICESat/GLAS instrument (Hyde et al., 2005). However, such fine resolution and accurate DEMs are not available globally. The experiment was repeated without a DEM and a canopy height accuracy (RMSE) of 3.8 m was achieved. This study was over predominantly flat ground with 55% of footprints on slopes less than 5° and only 6% over 15° (Rosette pers comms). The errors were not given as a function of slope angle and so it is not clear how well the pure Gaussian decomposition performed over slopes.

Lefsky et al. (2005) used ICESat/GLAS to study an area with slopes between 10° and 20°. They achieved a canopy height accuracy (RMSE) of 12.6 m using the 90 m horizontal resolution, near global shuttle radar topography mission (SRTM) DEM (Farr and Kobrick, 2000). Los et al. (2011) derived a global height with ICESat. They found RMSEs of between 7.1 m (over a flat site) and 42.3 m over more complex terrain. By filtering out all slopes over 10° (as well as more stringent cloud and minimum canopy cover checks) the RMSEs were reduced to between 4.1 m and 15.2 m.

Due to the difference in forests these three studies are not directly comparable, but it can be seen that canopy height errors over slopes are currently rather high and so there is room for a more accurate method.

A method for measuring canopy height accurately over steep topography is needed. Ideally the method would require no ground calibration or rely on any non-global datasets. It would be best to
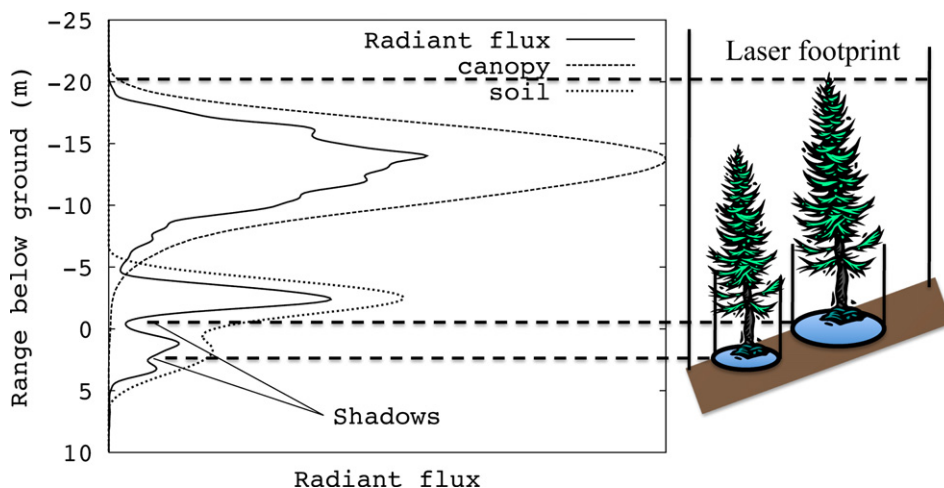

Fig. 4. Heterogeneity of a forest causing shadows and the subsequent deviation of features from simple analytical models.
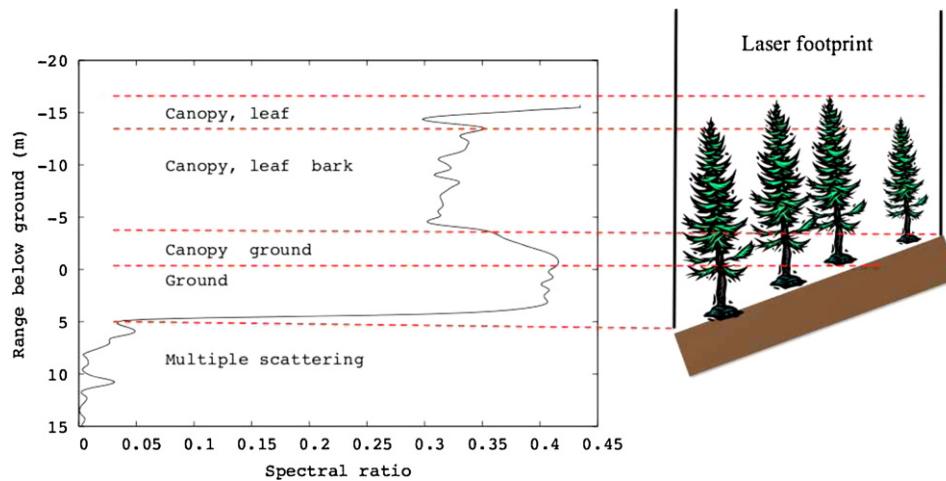
Fig. 5. Dual-wavelength waveform features. The spectral ratio is 550 nm over 850 nm.

avoid relying on any external data as that may suffer from geolocation issues. There is not a DEM with high enough resolution to determine slopes at the 30 m footprint scale with good accuracy beneath forests to accurately determine the proportion of the world's forests affected by steep topography, but previous studies have said it is not insignificant Takahashi et al. (2005).

1.3. Proposed dual-wavelength lidar

It is likely that the ground and vegetation will have different spectral properties (through different material compositions and structures) and so it is proposed that it will be possible to see the changing proportions of canopy and ground with a dual-wavelength lidar and so derive canopy height over topography more accurately.

Due to the energy requirements (particularly from space) only limited numbers of wavelengths have been considered for operational remote instruments (Morsdorf et al., 2009). Two wavelengths should be sufficient to detect the change of materials, though there have been recent advances towards hyper-spectral lidar (Kaasalainen et al., 2007). We propose that a dual wavelength lidar could feasibly be launched as a second generation canopy lidar satellite and will overcome the shortcomings of monochromatic lidar over topography.

1.3.1. Spectral ratio

The spectral ratio (waveform at one wavelength divided by that at another) should allow the ground to be identified through the issues caused by topography, short vegetation and shadowing described above. Fig. 5 shows a simulated spectral ratio over a Sitka spruce canopy on steep topography, similar to that in Fig. 2. The less intense waveform has been divided by the more intense to prevent large values as the less intense waveform approaches zero. This is similar to the vegetation index profiles of Morsdorf et al. (2009) but can be made especially sensitive to the canopy-ground transition.

1.4. Research questions

This paper investigates;

1. Whether such an instrument can be used to reliably separate canopy from ground over steep topography (30° slope) and a range of canopy densities and vertical structures? This separation of ground from canopy is the first step of any physically based lidar measurement.

2. Resulting tree height accuracies are compared to literature values from investigations with real monochromatic lidar; the "state of the art".

As yet there is no large-footprint, dual wavelength, waveform lidar capable of measuring forests from above and so a simulator is required. ICESat was dual wavelength, but the 532 nm channel was binned into 75 m intervals making it useless for canopy measurements (Harding, pers comms 2008). All the studies using real data mentioned in this paper suffered from confounding errors caused by geolocation mismatches and errors in the "truth". With a computer simulator the truth is known exactly and additional information can be recorded to help trace the source of errors and better understand the signal.

2. Method

The Monte-Carlo ray tracer of Lewis (1999) was modified to create a full waveform lidar simulator for any combination of wavelengths and sensor characteristics. The original ray tracer was validated as part of the RAdiation Model Intercomparison (RAMI) exercises (Pinty et al., 2004; Widlowski et al., 2007) and now forms part of the "surrogate truth" used to test all models against (Widlowski et al., 2008). The simulator has been compared to observations at a range of scales (from metres to hundreds of metres) and found to agree well (Disney et al., 2006, 2008). It has also been used to simulate lidar instruments (Disney et al., 2010; Hancock et al., 2011).

Explicit geometric forest models, in which the position, orientation and spectrum of every tree, branch, twig and leaf are described, were used. Their creation using the "Treegrow" program and other studies using them have been described in Disney et al. (2006), Disney et al. (2008) and Disney et al. (2010). Briefly biological growth rules are used to simulate a forest's growth for a given set of environmental conditions (in this case taken from field data collected in Thetford, UK). The growth and death of branches are modelled, producing a biologically realistic tree model of a given age.

The Monte-Carlo ray tracer calculates the paths of light beams through these explicit forest models to produce realistic remote sensing signals. Using explicit models and ray tracing is very computationally expensive but makes fewer assumptions than more abstract methods (such as Ni et al. (1999) and North (1996)), avoiding the dangers of effective parameters which may not capture important physical processes (Widlowski et al., 2005). Light rays
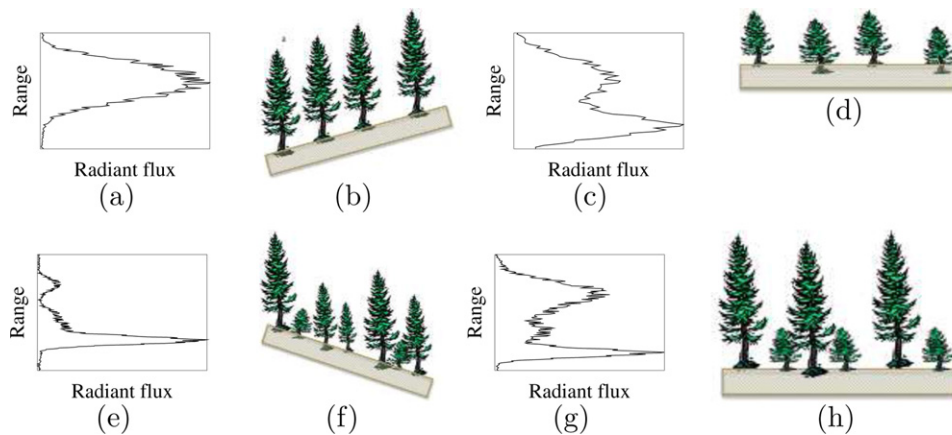
Fig. 6. Illustration of the range of forest models used. (a) Waveform for uniform mature on a slope. (b) Uniform mature on a slope. (c) Waveform for uniform young. (d) Uniform young. (e) Waveform for mixed age on a slope. (f) Mixed age on a slope. (g) Waveform for bimodal. (h) Bimodal. All waveforms are with a 7 ns laser pulse and include noise.

can scatter multiple times, adding to the recorded radiance and adding a slight range delay. In this study it was necessary to assume that all surfaces are Lambertian and that each material can be represented by a single reflectance and transmission spectrum.

Four unique individual Sitka spruce trees were generated for each of five age classes, with heights around 3 m, 9 m, 12 m, 20 m and 25 m (producing twenty separate trees). Clones of these were placed at random locations on a flat, sloped plane of soil or grass with different densities and combinations of age classes. A minimum separation between trees of 2 m was enforced. Trees were randomly rotated in azimuth and shifted downwards by up to 50 cm to prevent identical trees aligning. The resulting forests had canopy covers from 0.1% to 99.999% (within a 30 m footprint). The different combinations of age classes and slope are illustrated in Fig. 6 along with resulting waveforms. Forest models covered all combinations of density, age mixtures and ground slopes.

Onyx tree (Onyx Computing Inc, 2009) was used to create four individual birch trees (all of the same age class, around 4 m tall) (Disney et al., 2010). These were used to create forests in the same way as the Sitka spruce trees, though without the range of vertical structures.

Topography was included by tilting a flat plane by an angle. This will not capture all topographic effects, such as boulders, rough ground and non-linear slopes, but Chen (2010) showed that slope was more significant than roughness and so we believe that a sloped plane will suffice for an initial study. Brenner et al. (2003) made a similar decision for their study. Unless otherwise stated all footprints were on 30° slopes, a very steep case.

Leaf spectra were created from the PROSPECT model (Jacquemoud and Baret, 1990), a bark spectrum was taken from the LOPEX database (Hosgood et al., 1994) and a soil spectrum was created from the model of Price (1990). These are shown in Fig. 7. The LOPEX database was used to investigate possible ranges of these spectra and these ranges were used to find suitable laser wavelengths (see Section 2.2).

Real lasers have a finite pulse duration, blurring the resulting waveform and this is included as described in Hancock (2010, Section 4.1.4). Instrument noise was included in the simulated waveforms using the equations of Baltsavias (1999) and the values given in Hancock et al. (2008). To summarise, after a waveform has been created over a forest model with a given pulse length, the intensity value at each range bin and wavelength have a separate noise value added. Background noise was represented by a random number chosen from a uniform distribution and photon noise was represented by a random number chosen from a Gaussian distribution. The intensity was not allowed to go negative.

This tool allows the creation of simulated waveforms over a given forest (birch or Sitka spruce) that are equivalent to real measurements (a visual comparison with real data confirms this) so that inversion algorithms can be tested. Further, comprehensive, details of the simulator and the efforts taken to produce realistic data are given in Hancock (2010, chapter 4).

2.1. Spectral information

The spectral ratio waveform in Fig. 5 has five distinct sections. The initial peak in spectral ratio with a sharp drop-off due to the initial dominance of leaf in the canopy and because multiple scattering has not started to contribute. The ratio decreases through the canopy as it gets woodier and multiple scattering increases. It then changes as the ground starts to contribute, the direction of change depending on the relative reflectances of the canopy and ground at the two wavelengths; in this case it increases. The gradient of the change will depend upon the density of the foliage at the point at which the beam starts to intercept the ground, the denser the foliage the more gradual the transition. Once the foliage stops contributing the ratio flattens off to the pure ground value. The length of this section is controlled by the height from the ground to the bottom of the crowns. Finally, the spectral ratio drops as only multiple scattering echoes are left (if the lower reflectance waveform were the denominator this would approach infinity).

The spectral ratio is controlled by the material single scattering albedo, the proportion of each of those materials, the multiple scattering contributions and the phase function. The simulator was used to explore the behaviour of each of these variables through a forest canopy (shown in Fig. 8). An infinitely short laser pulse and no noise was used to make the canopy properties clearer. Again the less intense waveform has been divided by the more intense. The proportions of leaf, wood and soil will change through a canopy; in the absence of multiple scattering each material will contribute to the measured intensity by its projected area multiplied by its albedo and phase function. here phase function is defined as the factor scaling hemispherical albedo of a material to the albedo for a particular viewer-illumination geometry). Fig. 8(c) shows that the canopy starts off leafy, becoming woodier towards the ground, though with some heterogeneity. Interestingly some canopy (almost entirely wood) is visible almost to the bottom of the waveform.

Fig. 8(d) shows that there is no general trend in the phase function, except for wood higher up in the canopy where Fig. 8(c) shows it is predominantly leaf and so this is unlikely to be significant. The spectral ratio was calculated with and without multiple scattering. The intensity of multiply-scattered light is attenuated by the single
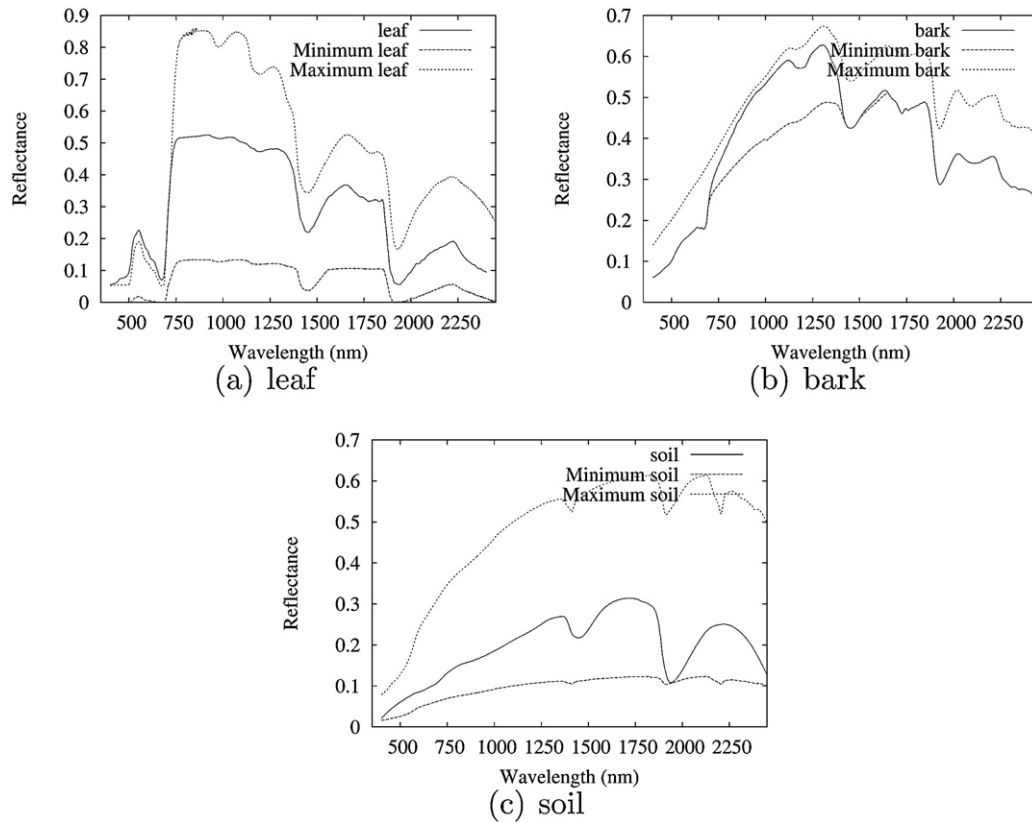
Fig. 7. Element spectra used with minimum and maximum values of observations.

scattering albedo to the power of the number of interactions and so the more intense waveform should have a much greater multiple scattering contribution. Fig. 8(e) shows this to be the case. In addition scattering adds heterogeneity to the signal and causes a slight decrease in the ratio with range. Interestingly, the two ratios are similar towards the top, indicating that multiple scattering has not started to contribute by then, due to the introduction of a range delay (a few tens of centimetres). It may be possible to use the range before the initial drop to determine the multiple scattering delay and so learn more about the structure through re-collision probability (Huang et al., 2007). This was not pursued in this paper.

2.2. Wavelength selection

All simulations over Sitka spruce and birch canopies showed similar trends and so these will be taken as general. The feature of interest is a change in spectral ratio between the pure-canopy and ground-with-canopy section and the wavelengths should be chosen to accentuate this. A number of criteria for selecting wavelengths can be set.

The less intense waveform should be divided by the more intense, therefore;

$$\rho_{\omega,canopy} > \rho_{\lambda,canopy} \tag{1}$$

$$\rho_{\omega,ground} > \rho_{\lambda,ground} \tag{2}$$

where $\rho_{\omega,canopy}$ is the canopy reflectance at the denominator wavelength, ω. $\rho_{\lambda,canopy}$ is the canopy reflectance at the numerator wavelength, λ. $\rho_{\omega,ground}$ and $\rho_{\lambda,ground}$ are the same for the ground (set as pure soil here). Here canopy reflectance at a particular wavelength is the weighted average of leaf, $\rho_{\lambda,leaf}$, and bark, $\rho_{\lambda,bark}$, reflectance; $\rho_{\lambda,canopy} = k\rho_{\lambda,leaf} + (1-k)\rho_{\lambda,bark}$, where k lies between

0 and 1 and varies with height and location. This ignores structural effects but is sufficient for an initial wavelength selection.

As multiple scattering increases with range (Fig. 8(e)), the spectral ratio will decrease towards the canopy bottom. This cannot be changed given the above criteria and so the canopy to ground transition will be more apparent if the change caused by an increasing wood fraction (Fig. 8(c)) also causes a decrease in the ratio and the ground has a higher spectral ratio than the canopy. These criteria can be phrased as;

$$\frac{\rho_{\lambda,leaf}}{\rho_{\omega,leaf}} > \frac{\rho_{\lambda,bark}}{\rho_{\omega,bark}} \tag{3}$$

$$\frac{\rho_{\lambda,canopy}}{\rho_{\omega,canopy}} < \frac{\rho_{\lambda,ground}}{\rho_{\omega,ground}} \tag{4}$$

The spectral contrast was calculated using a range of reflectances between the minimum and maximum values from the LOPEX database (Hosgood et al., 1994), the prospect model (Jacquemoud and Baret, 1990) and spectra collected with an ASD FSPro spectrometer (ASD inc., Boulder, CO, USA) in Kruger National Park. All spectra were between 400 nm and 2500 nm sampled every 10 nm (shown in Fig. 7). A range of canopy reflectance values were calculated by varying k between 0 and 1. A spaceborne instrument will suffer from atmospheric absorption and so this must be taken in to account. The ATRAN model (Lord, 1992) was used with the default parameters to calculate the atmospheric transmission between 850 nm and 2500 nm. The transmission was assumed to be unity between 450 nm and 850 nm. A compiled version of ATRAN is available to run online (SOFIA, 2010).

The best spectral contrast was achieved for all possible canopy compositions using 492 nm as the numerator and 1,112 nm as the denominator, giving a mean spectral contrast of 0.33. At these wavelengths the element reflectances were between 5.8% and 15%. This can be raised to be between 6.4% and 21% by using 512 nm
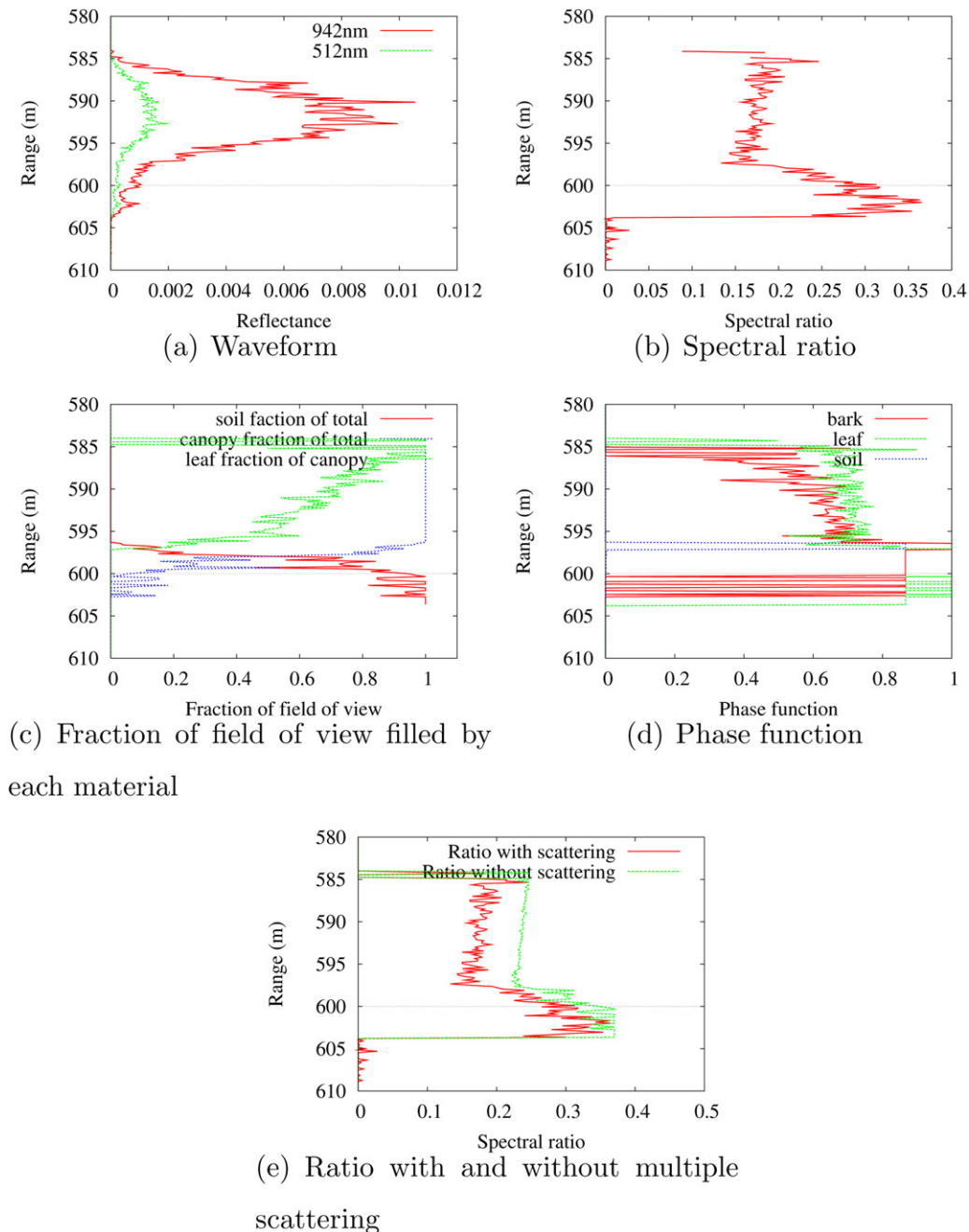
Fig. 8. Factors contributing to the spectral ratio (512 nm over 942 nm) of a 16 m tall Sitka spruce forest with 90% canopy cover on a 30° slope from simulation. The line at 600 m shows the centre of the ground which extends 3.5 m above and below. (a) Waveform; (b) spectral ratio; (c) fraction of field of view filled by each material; (d) phase function; (e) ratio with and without multiple scattering.

over 942 nm, which has a spectral ratio of 0.31. A higher reflectance would be an advantage and so 512 nm over 942 nm will be used for the rest of this paper unless otherwise stated. Whether or not suitable laser sources are available at these wavelengths is beyond the scope of this paper.

2.2.1. Grass covered floor

The previous section assumed a pure soil background. However it is possible that the background may be grass, moss or other vegetation. A worst case scenario would be for it to have the same element reflectance as the tree leaves. The two spectra would still not be identical due to the mixture of wood in the canopy and structural effects. The ray tracer was used to determine the canopy spectrum (taking structure into account) and the above wavelength selection analysis repeated.

For a pure grass background 512 nm over 942 nm has a spectral contrast of 0.034, around a tenth of that for a soil background. The optimum wavelengths would be 500 nm over 1890 nm, giving a spectral contrast of 0.59. This is higher than the soil ground contrast as structural effects in the canopy (multiple scattering and phase function) were not taken into account then. Therefore, even when the ground has exactly the same spectrum as leaves there is still a spectral contrast due to the mix of wood and structural effects in the canopy. It is very unlikely that the composition of the ground and canopy, spectrally and structurally, will lead to exactly the same spectra. Therefore there should always be two wavelengths which will show a spectral contrast over a surface.

It may not be possible to find two wavelengths that satisfy these criteria over all land surface types, but a global analysis of land cover is beyond the scope of this paper as it is meant as a proof of concept.

2.3. Information extraction

With the above criteria the start of the ground signal will be marked by a sharp increase in the spectral ratio. This may not necessarily be marked by a minimum in the spectral ratio but there will always be a maximum of the second derivative.

Noise and heterogeneity will cause spikes, particularly in the higher order derivatives and so some form of smoothing is required. Convolution with a Gaussian was selected for this study. The algorithm should aim to smooth away all maxima of the second derivative except the one of interest (start of the ground). At the same time the function should be as narrow as possible to minimise the shifting of features. Therefore the finest possible Gaussian that leaves a single maximum of the second derivative was used (found by iterating with different Gaussian widths) and the last remaining maxima of the second derivative taken as the start of the ground return. For the waveforms tested, a 2 m to 10 m long Gaussian was needed, with it generally lying around 3 m long. Convolution with a Gaussian will spread the signal into previously empty areas, producing meaningless spectral ratios. These tails can be avoided by applying the cumulative energy threshold of Hofton et al. (2000) and ignoring all signal outside of that. Smoothing the individual waveforms before calculating the spectral ratio will minimise the impact of noise.

At the beginning and end of the signal there will be rapid changes in the spectral ratio and so its derivatives. These "wings" could obscure the ground and so only the signal between the first minimum of the second derivative (leading wing) and the last minimum of the second derivative (trailing wing) should be searched. Under certain conditions this may truncate the features of interest (very low or high canopy covers) and steps should be taken to avoid this.

2.3.1. Edge preservation

The start of the ground return will be shifted upwards by any smoothing, introducing bias. Decreasing the smoothing function width in areas of interest and increasing it elsewhere will help reduce this bias (DaSheng, 1993). Weighting the function's width by the gradient of the spectral ratio (the greater gradient the narrower the function) should preserve the position of the ground. To avoid noise the weighting should be based on a smoothed spectral ratio. The weighting, w, was related to the gradient of the spectral ratio, $grad$ by;

$$w = \frac{1}{b(|grad| - a)} + c \qquad (5)$$

where a, b and c are constants set by the minimum and maximum smoothing to be used. The conditions and resulting values for a, b and c are given in Appendix A. This form was chosen to give an asymptote to cope with very steep gradients in the spectral ratio. It is somewhat arbitrary and should be refined in future studies.

2.4. Experimental design

The simulator was used to create a library of 1600 dual wavelength waveforms over a range of forest densities, structures and 30° slope for Sitka spruce with a soil background. Each waveform had different sets of noise of the same level applied (different random number seeds) to produce 16,000 "measured" waveforms. All simulations used a range resolution of 15 cm, a laser pulse length of 8 ns (full width half maximum, FWHM, 2.4 m long) and a 30 m footprint; similar to the recently cancelled DEDynI (Dubayah et al.,
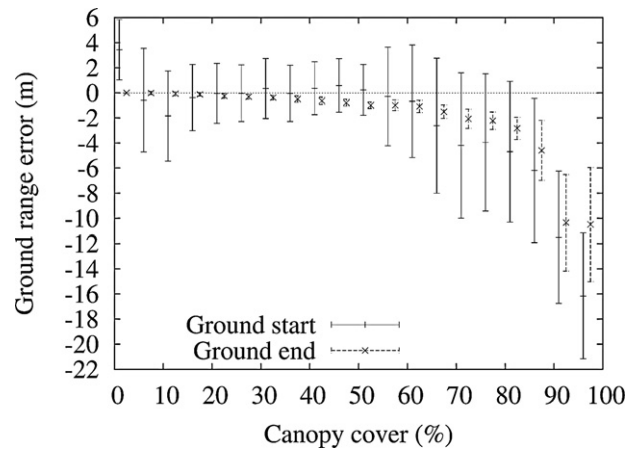
Fig. 9. Ground range error against canopy cover for Sitka spruce forests on a 30° slope using the spectral ratio method with 512 nm over 942 nm, 30 m footprint, 15 cm range resolution and an 8 ns laser pulse. Error bars show one standard deviation.

2008). The optimum wavelengths over soil, 512 nm over 942 nm, were used. As an independent test the analysis was repeated over birch, which had played no part in the algorithm development.

The analysis was repeated with a grass covered floor using 512 nm over 942 nm (the optimum for soil) and repeated with 500 nm over 1890 nm (the optimum for grass) to see if the method is tolerant to vegetation covered floors.

To provide a direct comparison to studies using real data (Lefsky et al., 2005; Los et al., 2011) the analysis was repeated using ICESat like parameters. A 65 m footprint, 7 ns laser pulse (Zwally et al., 2002), but using the dual wavelengths (512 nm over 942 nm). The noise tracking method described in Hancock et al. (2011) was used to determine the tree tops and the canopy height taken as the height of this above the mean ground position. It is impossible to tell where the tallest tree lies within a footprint and so tree height over a slope is not easily measured with large footprint lidar (Los et al., 2011). The 12.6 m RMSE achieved by (Lefsky et al., 2005) was taken as the benchmark accuracy over steep slopes (that study used an external DEM).

3. Results

The errors for determining the start and end of the ground return are given in Fig. 9. Here error is the estimate minus the truth, so a negative value is an underestimate. Unsurprisingly the end of the ground return is accurately determined until higher (>85%) canopy covers though the errors become quite large above 90% cover. As canopy cover increases the ground return is weakened and so is more likely to be lost in noise.

The start of the ground has proven harder to determine. For sparse (<10% canopy cover) the canopy return is very weak and likely to be lost in the noise removal operations. In the absence of the true canopy to ground transition, variations in multiple scattering intensity and canopy composition may be taken as the start of the ground return, leading to an overestimate of range. For very dense (>90% canopy cover) forests the opposite is true, a weak ground return being lost leading to an underestimate of range. Above 80% canopy cover there was an increase in the spread and bias of errors. This is due to the canopy structure and will be examined in more detail in Section 3.1. The overall RMSE in the range to the start of the ground signal was 3.2 m with a mean bias of −1.3 m. Limiting this to canopies with covers below 99% reduced the RMSE to 2.7 m and the bias to 67 cm.
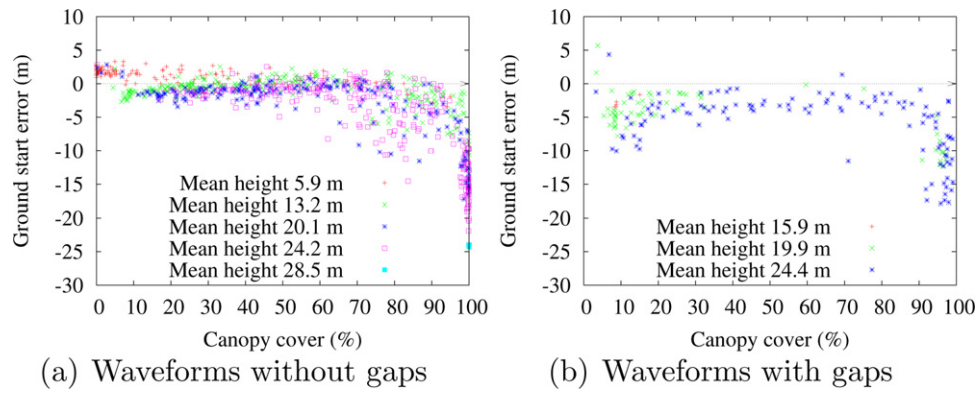
Fig. 10. Ground-start range error against canopy cover split by mean maximum canopy height using the spectral ratio method with 512 nm over 942 nm, 30 m footprint, 15 cm range resolution and an 8 ns laser pulse. (a) Waveforms without gaps and (b) waveforms with gaps.

For a vegetation covered floor the ground start position was determined with an RMSE of 2.26 m with a bias of −75 cm using 512 nm over 942 nm and 1.79 m with a bias of −19 cm using 500 nm over 1890 nm. Both of these are comparable to the soil covered ground results. Therefore it seems that unless the particular combination of canopy and ground materials and structural effects happen to give the two exactly the same spectra, two wavelengths can be found that allow the method presented here to be used and errors are not greatly increased by using non-optimum wavelengths. Due to the very different structural effects of a complex 3D canopy and the ground we feel this situation is very unlikely. The same two wavelengths may not be appropriate for all land cover types (e.g. moss and soil covered ground) and so an operational instrument may need more than two wavelengths to ensure global operation.

The results for birch were very similar to those for Sitka spruce forests with similar canopy covers. This suggests that the method is tolerant to different species, though experiments with more models would be needed to say for certain. The analysis was repeated with an infinitely short laser pulse (impossible in reality) and this gave very similar results for the ground-start errors. This suggests that the method is insensitive to laser pulse length.

The edge preserving method described in Section 2.3.1 adds computational expense. To justify this the analysis was repeated without it. The ground start RMSEs were found to be the same, however the bias was greater (roughly 1 m). Therefore we believe it is worth the computational expense.

3.1. Vertical structure

Fig. 10 gives the errors in ground-start position separated by canopy height (binned by maximum height within a footprint) and into canopies with clear gaps somewhere in the waveform (as in Figs. 1 and 3) and those without (as in Fig. 2). Only a single set of noise was added and inversions performed on each waveform to make the graphs clearer (1600 waveforms). This shows that the method performed worse with "gappy" waveforms. Duncanson et al. (2010) found a similar result in which their method performed better for forests on slopes of certain angles.

In a "gappy" waveform, the ground-start can be on either side of the gap and then either at the gap (as in Fig. 1) or within the signal (Fig. 3). The method presented here did not try to take gaps into account and so struggled in these cases. Smoothing could easily cause the transition feature to jump over a gap, amplifying the error. The feature will always be shifted upwards (away from the ground) by smoothing and so these errors are negative. It should be possible to overcome this by either closing the gaps during analysis and keeping track of where they lie or some form of classification of

the spectral ratio values, though there was not time to explore this within this project.

For forests without clear gaps in the canopy a number of different cases are apparent. The same trends for sparse (<10%) and dense (>98%) canopies discussed in the last section were evident. Above 60% cover there are a number of large underestimates of up to 10 m. There are not enough to greatly increase the spread and bias in Fig. 9 and so this may be acceptable. Examination of the waveforms reveals that these cases have sections of very low intensity within the signal and so are more readily affected by noise. Thus they are almost "gappy" canopies and the improvements needed to apply the method to "gappy" canopies should also aim to correct for this.

Slopes other than 30° were simulated, however as slope decreases the number of gappy canopies increases, so more waveforms have the large errors shown in Fig. 10(b). Therefore we have not attempted to determine the dependence of error on slope, as errors caused by gaps in the canopy will dominate.

Short trees (<10 m tall) tended to show overestimates in range. This is most probably controlled by foliage density at the point at which the ground starts to contribute. The denser the canopy at this point the weaker the ground return will be, so the increase in spectral ratio from pure canopy to pure ground will be more gradual. For a given canopy cover, a shorter tree will have denser foliage closer to the ground, decreasing the ground return strength at the transition and so making it harder to determine its position. Changes in multiple scattering contribution and canopy composition may accidentally be interpreted as the ground-start position. Other than for trees less than 10 m tall, for a given canopy cover there was no relationship between canopy height and error, that being dominated by canopy cover and the vertical structure.

The experiments were repeated for all wavelength combinations that matched the above criteria, gave a spectral ratio above 0.2 and had element reflectances above 5%. All gave similar results with RMSEs of ground-start lying within 50 cm of each other. This suggests that a wide range of wavelengths may be suitable if suitable laser sources are not available at 512 nm and 942 nm and giving us some hope that a single pair of wavelengths can be found that will work over a broad range of ground spectra. A more comprehensive spectral analysis, beyond the scope of this proof of concept paper, would be needed.

3.2. Canopy height

For a dual-wavelength version of ICESat (512 nm and 942 nm) over sloped forests, canopy heights were obtained with root mean square errors of less than 4 m for all covers up to 90%. For canopy covers above 90% the errors increased to an average of 14 m with

some at very high covers (98% and higher) reaching 25 m. The RMSE over all canopy covers was 3.2 m with a mean bias of −1.96 m. This dropped to 2.03 m and a bias of −63 cm when ignoring canopies above 97% cover. The errors had a very similar dependence on canopy cover to those in Figs. 9 and 10 suggests that the error is not related to canopy height, only canopy cover and structure. To quantify this a straight line was fit to a scatterplot of ground start RMSE against canopy height for each canopy cover (10% cover bins). It was found that the fit of a straight, sloping line (RMSE depends on canopy height) was not significantly better than a horizontal line (RMSE does not depend on canopy height) and so we believe that vertical structure and canopy cover dominate the errors in this method. This method is much more accurate than the 12.6 m achieved in Lefsky et al. (2005), although it's not clear if the two sets of canopies are directly comparable.

In the absence of a real dual-wavelength lidar or a fully digitised area of forest where real and simulated measurements can both be collected, a more comprehensive comparison of monochromatic and dual wavelength lidar canopy height estimates cannot be performed. It is clear that dual wavelength lidar has an advantage in the three cases given in the introduction (Figs. 2–4).

4. Conclusions

The four possible combinations of canopy and ground returns in lidar signals have been highlighted; clear separation between the two (Fig. 1), no clear separation (Fig. 2), a break in the canopy with no separation between it and the ground (Fig. 3) and no separation between the ground and canopy with a drop in intensity within the ground return (Fig. 4). Except for the first case of clear separation, monochromatic lidar cannot accurately resolve the ground return in any of these cases, preventing physically-based measurement and leading to inaccurate estimates of biophysical parameters.

The potential of using dual wavelength, large-footprint, spaceborne lidar to separate ground and canopy returns, particularly in the presence of topography and understory vegetation, has been demonstrated. This first step is necessary for the physically-based measurement of any forest parameter and, as it relies only on the shape of the spectral ratio, will be robust to differences in scene reflectance, atmospheric conditions and variable instrument gain.

This paper has shown that the extra information contained in a spectral ratio (Fig. 5) can be used to develop a physically-based (and so globally applicable and consistent) method for measuring forests. All the results have been based upon simulated data, which has allowed a minute examination of the errors, but the method will need testing with real data once that becomes available. In particular it requires the ground to have a different spectral ratio to the canopy; whether it be made of soil, leaf, litter, grass or some combination of these.

Tests with a pure vegetation ground suggests that structural effects make it very unlikely that a canopy will have exactly the same spectrum as the ground beneath, and so it should be possible to find two wavelengths with a strong spectral gradient. These two wavelengths may not be the same over the globe (though RMSEs were comparable when using 512 nm over 942 nm over both soil and grass)) and so an operational satellite may need to be capable of producing more than two wavelengths, though only two at any one time. Further analysis with a broader range of spectra, their relative abundance on the land surface and their importance to various science questions is needed to select wavelengths for an operational instrument.

Simulations of a dual-wavelength ICESat like instrument gave lower errors than the 12.6 m reported by Lefsky et al. (2005) using the monochromatic ICESat. Therefore it is proposed that a dual wavelength lidar will allow more accurate measurement of forests on steep terrain than is possible with monochromatic lidar.

This paper has proven that dual-wavelength lidar can retrieve canopy height in the presence of topography and understory vegetation more accurately than monochromatic lidar, without the need for any external datasets. The method employed was somewhat arbitrary and some refinements are needed, particularly to allow it to deal with "gappy" waveforms.

Appendix A. Weighting function constants

The constants in Eq. (5) were set by forcing the smoothing function to have the greatest value at the smallest observed gradient ($w = smooth_{max}$, $\left|grad\right| = \left|grad\right|_{min}$), the minimum smoothing at the maximum gradient ($w = smooth_{min}$, $\left|grad\right| = \left|grad\right|_{max}$) and, to get a noticeable asymptote, the gradient of the function at $\left|grad\right|_{max}$ to be (an arbitrary) one hundredth of its value at $\left|grad\right|_{min}$. Solving for these conditions gives;

$$a = \frac{\sqrt{100}\left|grad\right|_{min} - \left|grad\right|_{max}}{\sqrt{100} - 1} \tag{A.1}$$

$$b = \frac{1}{(\left|grad\right|_{max} - a)(smooth_{min} - c)} \tag{A.2}$$

$$c = \frac{smooth_{min}(\left|grad\right|_{max} - a) - smooth_{max}(\left|grad\right|_{min} - a)}{\left|grad\right|_{max} - \left|grad\right|_{min}} \tag{A.3}$$

For this purpose, using $\sqrt{100} = +10$ gives the correct value for Eq. (A.1).

References

Baltsavias, E.P., 1999. Airborne laser scanning: basic relations and formulas. ISPRS Journal of Photogrammetry & Remote Sensing 54, 199–214.

Brenner, A.C., Zwally, H.J., Bentley, C.R., Csatho, B.M., Harding, D.J., Hofton, M.A., Minster, J.-B., Roberts, L., Saba, J.L., Thomas, R.H., Yi, D., 2003. Geoscience laser altimeter system. derivation of range and distributions from laser pulse waveform analysis for surface elevations, roughness, slope, and vegetation heights. Algorithm Theoretical Basis Document Version 4.1.

Chen, J.M., Cihlar, J., 1996. Retrieving leaf area index of boreal conifer forests using landsat TM images. Remote Sensing of Environment 55, 153–162.

Chen, Q., 2010. Retrieving vegetation height of forests and woodlands over mountainous areas in the pacific coast region using satellite laser altimetry. Remote Sensing of Environment 114, 1610–1627.

Clark, D.B., Mercado, L.M., Sitch, S., Jones, C.D., Gedney, N., Best, M.J., Pryor, M., Rooney, G.G., Essery, R.L.H., Blyth, E., Boucher, O., Harding, R.J., Huntingford, C., Cox, P.M., 2011. The Joint UK Land Environment Simulator (JULES), model description – Part 2: Carbon fluxes and vegetation dynamics. Geoscientific Model Development 4, 701–722.

DaSheng, F., 1993. A new formula for the linear constrained matrix inversion. In: Proceedings of IEEE Topical Symposium on Combined Optical, Microwave, Earth and Atmosphere Sensing, pp. 60–63.

Disney, M.I., Kalogirou, V., Lewis, P., Prieto-Blanco, A., Hancock, S., Pfeifer, M., 2010. Simulating the impact of discrete-return lidar system and survey characteristics

over young conifer and broadleaf forests. Remote Sensing of Environment 114, 1546–1560.

Disney, M.I., Lewis, P., Bouvet, M., July 2008. Quantifying surface reflectivity for spaceborne lidar missions. In: Geoscience and Remote Sensing Symposium, 2008. IGARSS 2008. IEEE International, vol. 2, pp. II-249–II-252.

Disney, M.I., Lewis, P., Saich, P., 2006. 3D modelling of forest canopy structure for remote sensing simulations in the optical and microwave domains. Remote Sensing of Environment 100, 114–132.

Dubayah, R., Bergen, K., Hall, F., Hurtt, G., Houghton, R., Kellndorfer, J., Lefsky, M., Moorcroft, P., Nelson, R., Saatchi, S., Shugart, H., Simard, M., Ranson, J., Blair, J.B., December 2008. Global Vegetation Structure from NASA's DESDynI Mission: An Overview. AGU Fall Meeting Abstracts, pp. H1+.

Dubayah, R.O., Drake, J.B., 2005. Lidar remote sensing for forestry applications. Journal of Forestry 98, 44–46.

Duncanson, L.I., Niemann, K.O., Wulder, M.A., 2010. Estimating forest canopy height and terrain relief from glas waveform metrics. Remote Sensing of Environment 114, 138–154.

Farr, T., Kobrick, M., May 2000. The shuttle radar topography mission: a global DEM. In: Proceedings of the 3rd European Conference on Synthetic Aperture Radar. Munich, Germany, EUSAR 2000.

Hancock, S., 2010. Understanding the measurement of forests with waveform lidar. Ph.D. Thesis. University College London, http://eprints.ucl.ac.uk/20221/.

Hancock, S., Disney, M., Muller, J.-P., Lewis, P., Foster, M., 2011. A threshold insensitive method for locating the forest canopy top with waveform lidar. Remote Sensing of Environment 115, 3286–3297.

Hancock, S., Lewis, P., Disney, M.I., Foster, M., Muller, J.-P., 2008. Assessing the accuracy of forest height estimation with long pulse waveform lidar through Monte-Carlo ray tracing. Silvilaser, Edinburgh, September 17–18.

Harding, D.J., Carabajal, C.C., 2005. Icesat waveform measurements of within-footprint topographic relief and vegetation vertical structure. Geophysical Research Letters 32, L21S10.

Hofton, M.A., Minster, J.B., Blair, J.B., 2000. Decomposition of laser altimeter waveforms. IEEE Transactions on Geoscience and Remote Sensing 38, 1989–1996.

Hofton, M.A., Rocchio, L.E., Blair, J.B., Dubayah, R., 2002. Validation of vegetation canopy lidar sub-canopy topography measurements for a dense tropical forest. Journal of Geodynamics 34, 491–502.

Hosgood, B., Jacquemoud, S., Andreoli, G., Verdebout, J., Pedrini, G., Schmuck, G., 1994. Leaf Optical Properties EXperiment 93 (LOPEX93). European Commission – Joint Research Centre, Ispra, Italy. EUR 16095 EN.

Houghton, R.A., Lawrence, K.T., Hackler, J.L., Brown, S., 2001. The spatial distribution of forest biomass in the Brazilian Amazon: a comparison of estimates. Global Change Biology 7, 731–746.

Huang, D., Knyazikhin, Y., Dickinson, R.E., Rautiainen, M., Stenberg, P., Disney, M., Lewis, P., Cescatti, A., Tian, Y., Verhoef, W., Martonchik, J.V., Myneni, R.B., 2007. Canopy spectral invariants for remote sensing and model applications. Remote Sensing of Environment 106, 106–122.

Hurtt, G.C., Dubayah, R., Moorcroft, P.R., Pacala, S.W., Blair, J.B., Fearon, M.G., 2004. Beyond potential vegetation: combining lidar data and a height structured model for carbon studies. Ecological Applications 14, 873–883.

Hyde, P., Dubayah, R., Peterson, B., Blair, J.B., Hofton, M., Hunsaker, C., Knox, R., Walker, W., 2005. Mapping forest structure for wildlife habitat analysis using waveform lidar: validation of montane ecosystems. Remote Sensing of Environment 97, 427–437.

Jacquemoud, S., Baret, F., 1990. Prospect: a model of leaf optical properties spectra. Remote Sensing of Environment 34, 75–91.

Kaasalainen, S., Lindroos, T., Hyyppa, J., 2007. Toward hyperspectral lidar: measurement of spectral backscatter intensity with a supercontinuum laser source. IEEE Transactions on Geoscience and Remote Sensing Letters 4, 211–215.

Lefsky, M.A., 2010. A global forest canopy height map from the moderate resolution imaging spectroradiometer and the geoscience laser altimeter. Geophysical Research Letters 37, doi:10.1029/2010GL043622.

Lefsky, M.A., Harding, D.J., Cohen, W.B., Carabajal, C.C., Espirito-Santo, F.D.B., Hunter, M.O., de Oliveira Jr., R., 2005. Estimates of forest canopy height and aboveground biomass using icesat. Geophysical Research Letters 32, doi:10.1029/2005GL023971.

Lefsky, M.A., Keller, M., Yong, P., de Camargo, P.B., Hunter, M.O., 2007. Revised method for forest canopy height estimation from geoscience laser altimeter system waveforms. Journal of Applied Remote Sensing 1, 1–18.

Lewis, P., 1999. Three-dimensional plant modelling for remote sensing simulation studies using the botanical plant modelling system. Agronomie 19, 185–210.

Lord, S.D., 1992. A new software tool for computing Earth's atmospheric transmission of near- and far-infrared radiation. Technical Report. Ames Research Centre, Moffett Field, California. NASA technical memorandum 103957.

Los, S.O., Rosette, J.A.B., Kljun, N., North, P.R.J., Suárez, J.C., Hopkinson, C., Hill, R.A., Chasmer, L., van Gorsel, Mahoney, C., Berni, J.A.J., 2011. Vegetation height products between 60°S and 60°N from ICESat GLAS data. Geoscientific Model Development Discussions 4, 2327–2363.

Morsdorf, F., Nichol, C., Malthus, T., Woodhouse, I.H., 2009. Assessing forest structural and physiological information content of multi-spectral lidar waveforms by radiative transfer modelling. Remote Sensing of Environment 113, 2152–2163.

Myneni, R.B., Hoffman, S., Knyazikhin, Y., Privette, J., Glassy, J., Tian, Y., Wang, S., Song, X., Xhang, Y., Smith, G.R., Lotsch, A., Friedl, M., Morsiette, J.T., Votava, P., Nemani, R.R., Running, S.W., 2002. Global products of vegetation leaf area and fraction absorbed par from year one of modis data. Remote Sensing of Environment 83, 214–231.

National Academy of Sciences, 2007. Earth Science and Applications from Space: National Imperatives for the Next Decade and Beyond. National Academies Press, http://www.nap.edu/catalog/11820.html.

Ni, W., Li, X., Woodcock, C.E., Caetano, M.R., Strahler, A.H., 1999. An analytical hybrid GORT model for bidirectional reflectance over discontinuous plant canopies. IEEE Transactions on Geoscience and Remote Sensing 37, 987–999.

North, P.R.J., 1996. Three-dimensional forest light interaction model using a Monte Carlo method. IEEE Transactions on Geoscience and Remote Sensing 34, 946–956.

Onyx Computing Inc., 2009. Onyx tree professional. www.onyxtree.com (accessed 13.06.09).

Pinty, B., Widlowksi, J.-L., Taberner, M., Gobron, N., Verstraete, M.M., Disney, M., Gascon, F., Gastellu-Etchegorry, J.-P., Jiang, L., Kuusk, A., Lewis, P., Li, X., Ni-meister, W., Nilson, T., North, P., Qin, W., Su, L., Tang, S., Thompson, R., Verhoef, W., Wang, H., Wang, J., Yan, G., Zang, H., 2004. Radiation transfer model intercomparison (rami) exercise: results from the second phase. Journal of Geophysical Research 109, D06210.

Price, J.C., 1990. On the information content of soil reflectance spectra. Remote Sensing of Environment 33, 113–121.

Rosette, J.A.B., North, P.R.J., Suarez, J.C., 2008. Vegetation height estimates for a mixed temperate forest using satellite laser altimetry. International Journal of Remote Sensing 29, 1475–1493.

Rosette, J.A.B., North, P.R.J., Suarez, J.C., Los, S.O., 2010. Uncertainty within satellite lidar estimations of vegetation and topography. International Journal of Remote Sensing 31, 1325–1342.

SOFIA, 2010. ATRAN program. http://atran.sofia.usra.edu/cgi-bin/atran/atran.cgi (accessed 7.07.10).

Takahashi, T., Yamamoto, K., Senda, Y., Tsuzuku, M., 2005. Estimating individual tree heights of sugi (cryptomeria japonica d. don) plantations in mountainous areas using small-footprint airborne lidar. Journal of Forest Research 10, 135–142.

Waring, R.H., Law, B., Goulden, M.L., Bassow, S.L., McCreight, R.W., Wofsy, S.C., Bazzaz, F.A., 1995. Scaling gross ecosystem production at Harvard forest with remote sensing: a comparison of estimates from a constrained quantum-use efficiency model and eddy correlation. Plant Cell Environment 18, 1201–1213.

Widlowski, J.-L., Pinty, B., Lavergne, T., Verstraete, M.M., Gobron, N., 2005. Using 1-D models to interpret the reflectance anisotropy of 3-d canopy targets: issues and caveats. IEEE Transactions on Geoscience and Remote Sensing 43, 2008–2017.

Widlowski, J.-L., Robustelli, M., Disney, M., Gastellu-Etchegorry, J.-P., Lavergne, T., Lewis, P., North, P., Pinty, B., Thompson, R., Verstraete, M., 2008. The rami on-line model checker (romc): a web-based benchmarking facility for canopy reflectance models. Remote Sensing of Environment 112, 1144–1150.

Widlowski, J.-L., Taberner, M., Bruniquel-Pinel, V., Disney, M., Fernandes, R., Gastellu-Etchegorry, J.-P., Gobron, N., Kuusk, A., Lavergne, T., Leblanc, S., Lewis, P.E., Martin, E., Mottus, M., North, P.R.J., Qin, W., Robustelli, M., Rochdi, N., Ruiloba, R., Soler, C., Thompson, R., Verhoef, W., Verstraete, M.M., Xie, D., 2007. Third radiation transfer model intercomparison (rami) excerise: documenting progress in canopy reflectance models. Journal of Geophysical Research 112, D09111.

Williams, M., 1996. A three-dimensional model of forest development and competition. Ecological Modelling 98, 73–98.

Zimble, D.A., Evans, D.L., Carlson, G.C., Parker, R.C., Grado, C.G., Gerard, P.D., 2003. Characterizing vertical forest structure using small-footprint airborne lidar. Remote Sensing of Environment 87, 171–182.

Zwally, H.J., Shutz, B., Abdalati, W., Abshire, J., Bentley, C., Brenner, A., Bufton, J., Dezio, J., Hancock, D., Harding, D., Herring, T., Minster, B., Quinn, K., Palm, S., Spinhirne, J., Thomas, R., 2002. Icesat's laser measurements of polar ice, atmosphere, ocean and land. Journal of Geodynamics 34, 405–445.